Molecular Crystals and Liquid Crystals

ISSN: 1542-1406 (Print) 1563-5287 (Online) Journal homepage: http://www.tandfonline.com/loi/gmcl20

Thermal Analysis, Calorimetric and Electrical Polarization Studies in Smectic X* Phase of Hydrogen-Bonded Ferroelectric Liquid Crystals

Nataraj Pongali Sathya Prabu & Mathukumalli Lakshmi Narayana Madhu Mohan

To cite this article: Nataraj Pongali Sathya Prabu & Mathukumalli Lakshmi Narayana Madhu Mohan (2015) Thermal Analysis, Calorimetric and Electrical Polarization Studies in Smectic X* Phase of Hydrogen-Bonded Ferroelectric Liquid Crystals, Molecular Crystals and Liquid Crystals, 606:1, 12-35, DOI: 10.1080/15421406.2014.909615

To link to this article: http://dx.doi.org/10.1080/15421406.2014.909615

Mol. Cryst. Liq. Cryst., Vol. 606: pp. 12–35, 2015

ISSN: 1542-1406 print/1563-5287 online
DOI: 10.1080/15421406.2014.909615

Thermal Analysis, Calorimetric and Electrical Polarization Studies in Smectic X* Phase of Hydrogen-Bonded Ferroelectric Liquid Crystals

NATARAJ PONGALI SATHYA PRABU
AND MATHUKUMALLI LAKSHMI NARAYANA MADHU MOHAN*

Liquid Crystal Research Laboratory (LCRL), Bannari Amman Institute of Technology, Sathyamangalam, Tamilnadu, India

Intermolecular hydrogen-bonded ferroelectric liquid crystals are isolated and characterized. Formation of hydrogen bond is evinced by Fourier Transform Infra-Red (FTIR) studies. Phases are confirmed by polarizing optical microscopic (POM) studies and further confirmed by Differential Scanning Calorimetry (DSC) thermograms. Phase diagram is constructed from POM and DSC data and the order of transition possessed by the individual phases are evaluated from the Cox parameter. Summation of the enthalpy values exhibited by the individual complexes both in heating and cooling cycles are compared to verify the thermal equilibrium exhibited by the system. Mono variant smectic X phase observed in two complexes are confirmed to be smectic ordering from the tilt angle, helix, and spontaneous polarization measurements. Enhancement of smectic X* thermal range is noticed through the phase diagram of the binary mixtures. Unwinding of the helix is measured from helical pitch measurements. From dielectric studies, the threshold values for two field-induced phase transitions E_1 and E_2 are measured. Electric field–temperature (E–T) phase diagram is constructed from the threshold field values obtained with respect to the temperature variation. Further, molecular modeling is proposed for the observed electric field-induced phase transitions.*

Keywords Binary mixtures; field-induced phase transition; hydrogen-bonded ferroelectric liquid crystals; smectic X* phase; spontaneous polarization

Introduction

Liquid crystals, the captivating materials have gained utmost importance in recent years due to their wide commercial viabilities [1, 2]. This fascinating fact made the noble researchers all around the sphere [3–10] to contribute their excellence [11–14] in producing various types of liquid crystals in different forms as per the required application needs. Among various routes existing in preparing different forms of liquid crystals, hydrogen-bonded liquid crystals [15, 16] yields a great interest in forming novel liquid crystalline materials, due to their ease of expanding the rigid rod segment of individual components, thus leading to the

*Address correspondence to M. L. N. Madhu Mohan, Liquid Crystal Research Laboratory (LCRL), Bannari Amman Institute of Technology, Sathyamangalam 638 401, Tamilnadu, India. E-mail: mln.madhu@gmail.com

Color versions of one or more of the figures in the article can be found online at www.tandfonline.com/gmcl.

formation or inducement of new liquid crystalline phases [17] which retains its chemical as well as thermal stability. Molecular reorganization and self-assembly capabilities of hydrogen bond, opened a new chapter in the development of liquid crystals, thus paving way for designing, synthesizing, and characterizing a numerous inter molecular hydrogen-bonded materials [18–23].

It is well known that mesogenic nature may exists between any two chemical moieties which may be either mesogenic [24–26] or nonmesogenic [27, 28] depending on the synthesis procedure. As benzoic acid is the prime component in formation of liquid crystalline materials through hydrogen bonding [17], in the present work Malic acid (MA) which is nonmesogenic in nature and various alkyl benzoic acids (nBA, n varies from ethyl to octyl) mesogenic in nature [24] are taken as the chemical moiety ingredients. Malic acid has the carbon atom which is surrounded by four different asymmetric groups leading it to be chiral carbon, it makes the product to be ferroelectric in nature. Seven such homologues (MA + nBA) are prepared by varying the alkyl carbon length from ethyl to octyl.

From our previous experience [23–26] it is noticed that new phases like smectic X [23, 29–33] and smectic R [26, 34] are induced in HBLC along with the conventional phases. It is interesting to note that in the present MA+nBA homologous series, a new smectic ordering labeled as smectic X* is identified. Hence, to understand its nature and response to the different parameters a thorough investigation such as optical, electrical, and thermal parameters are made on smectic X* phase, to confirm this phase to be a smectic one, tilt angle, the primary order parameter [35] is measured with respect to temperature and with different applied field. The unwinding of the helix is clearly noticed in the helical pitch measurements, thus confirming smectic ordering X* to be chiral. The enhancement of thermal range of this smectic ordered X* phase is further investigated by varying the molar ratio percentage of the complex exhibiting smectic X* phase with the other complex which does not exhibits smectic X* phase, [36]. The phase diagram for the binary mixture is constructed and the thermal range exhibited by smectic X* phase is deduced.

From electrical investigations, field-induced phase transitions [37, 38] are observed in smectic X* phase, from which the threshold stimuli value and optical extinction values are derived. A molecular modeling is proposed for optical extinction. E–T (Electric field against Temperature) diagram [38] clearly portraits the field-induced phase transitions (E_1 and E_2). Spontaneous polarization [39, 40], dielectric measurements are made in smectic X* phase for two homologues. Thus, a successful attempt is being made in investigating the occurrence and characterizing ferroelectric smectic X* phase.

Experimental

Observations of optical textures are made with a Nikon polarizing microscope (Nikon, Japan) equipped with Nikon digital CCD camera system with 5 mega pixels and 2560 × 1920 pixel resolutions. The liquid crystalline textures are analyzed and stored with the assist of NIS imaging software. The liquid crystal sample, in its isotropic state, is filled by capillary action into a commercially available polyamide buffed cell (Instec, USA) of 10 μm spacer. Temperature control of the liquid crystal cell is equipped with HCS402-STC 200 temperature controller (Instec, USA) to a temperature resolution of $\pm 0.1^{\circ}$C. This unit is interfaced to a computer by IEEE – STC 200 to control and monitor the temperature. Spontaneous polarization is measured with current repolarization method [39, 40] and the corresponding current profiles are recorded and analyzed with DSO (GW Instek GDS-2302A, Taiwan). Transition temperatures, corresponding enthalpy values and height

of the DSC peaks, are obtained by DSC (Shimadzu DSC-60, Japan) and TA-60-associated software. Dielectric measurements are carried out with low-frequency impedance Analyzer (Agilent 4192 A). MA and *p-n*-alkyl benzoic acids (nBA) are supplied by Sigma Aldrich, (Germany) and all the solvents used are of High Performance Liquid Chromatography (HPLC) grade.

Results and Discussion

Synthesis of HBLC

All the inter hydrogen-bonded ferroelectric liquid crystalline complexes examined in the present study are obtained by mixing two moles of *p-n*-alkyl benzoic acid (nBA, where $n = 2$ to 8) with one mole of MA in excess DMF and reprecipitating after the evaporation as reported in literature [41–43], the series is referred as MA+nBA. Molecular structure of the present hydrogen-bonded ferroelectric liquid Crystal (HBFLC) is presented as Fig. 1.

HBFLC complexes, of MA+nBA, isolatedunder the present investigation are white crystalline solids and are stable at room temperature (30°C). They are insoluble in water and sparingly soluble in common organic solvents such as methanol, ethanol, benzene, and dichloro methane. However, they show a high degree of solubility in coordinating solvents like dimethyl sulfoxide (DMSO), dimethyl formamide (DMF), and pyridine. They melt at temperatures below 138.8°C (Table 1) and show high thermal and chemical stability when subjected to repeated thermal scans performed during Polarizing Optical Microscopy (POM) and Differential Scanning Calorimetry (DSC) studies.

Phase Variance

Phase identification,transition temperatures, and the corresponding enthalpy values obtained in cooling and heating cycles of MA + nBA homologues are presented in Table 1. Transition temperatures observed in DSC are in concurrence with corresponding POM data.

Mesogenic Nature of MA + nBA. Mesogensof MA + nBA homologousseries are found toexhibit characteristic textures, [44], viz., cholesteric (Ch*) (schlieren brushes, plates 1 and 2), smectic X* (worm like texture, plate 3), and smectic G* (smooth multi colored mosaic like texture, plate 4). In addition, two more electric field-induced phases transitions labeled as E_1 (plate 5) and E_2 (plate 6) are observed which will be discussed in electric field-induced phase transition section. Parachromatic changes(from green color to red color) in cholesteric texture of MA + 7BA are depicted as plates 1 and 2. The change of refractive index with temperature leads to these parachromatic changes. General thermal

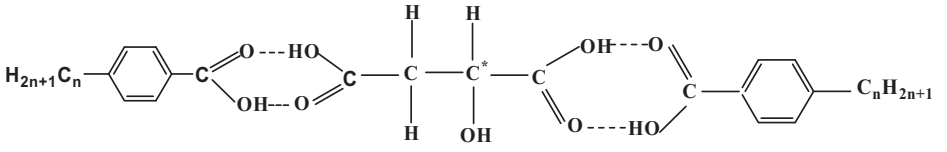

Figure 1. Molecular structure of MA+nBA homologous series.

Table 1. Transition temperatures and enthalpy values obtained by various techniques for MA+nBA homologous series

Complex	Phase variance	Technique	Crystal to melt	Ch	X*	G*	Crystal
MA+2BA	G*	DSC (h)	105.9 (48.96)			#	
		DSC (c)				102.3 (0.31)	100.3 (43.76)
		POM (c)				102.6	100.5
MA+3BA	G*	DSC (h)	138.8 (51.37)			#	
		DSC (c)				136.8 (1.83)	131.3 (47.63)
		POM (c)				137.1	131.6
MA+4BA	G*	DSC (h)	97.3 (49.89)			#	
		DSC (c)				100.6 (1.75)	89.3 (43.16)
		POM (c)				100.9	89.4
MA+5BA	X*	DSC (h)	87.8 (29.78)		#		
		DSC (c)			108.1 (0.78)		82.00 (28.77)
		POM (c)			108.4		82.2
MA+6BA	X*	DSC (h)	95.4 (29.32)		#		
		DSC (c)			98.8 (3.54)		86.8 (29.09)
					99.1		86.9
MA+7BA	Ch	DSC (h)	100.9 (37.43)	#			
		DSC (c)		104.00 (0.97)			94.4 (35.37)
		POM (c)		104.3			94.6
MA+8BA	Ch G*	DSC (h)	100.1 (40.88)	110.0 (2.96)		#	
		DSC (c)		110.0 (2.13)		106.5 (4.09)	93.00 (36.30)
		POM (c)		110.5		106.8	93.1

(h) heating run (c) cooling run.
#Monotropic transition.

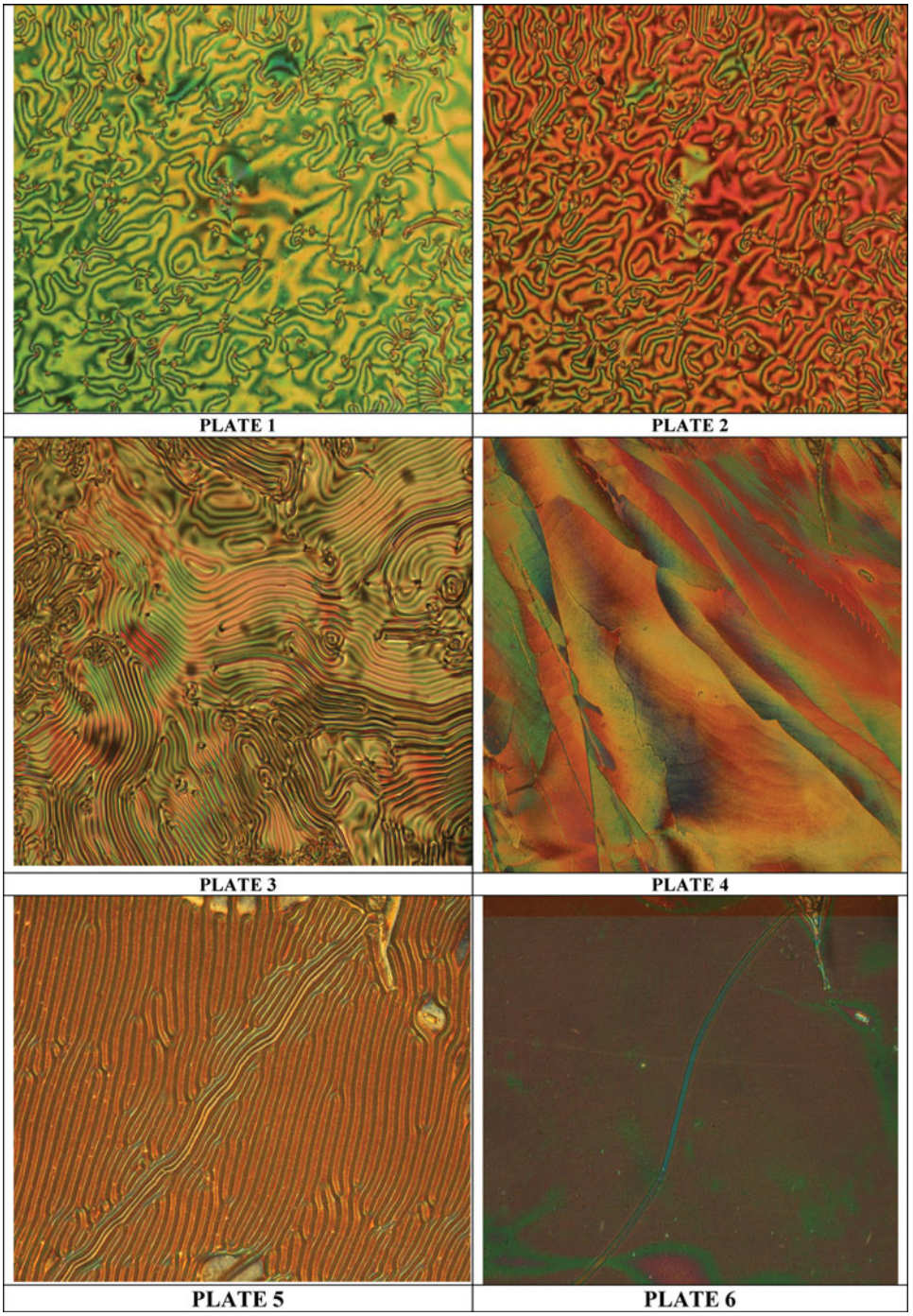

Plate 1. Schlieren brushes texture of cholesteric in MA+7BA; **2.** Parachromatic changes in cholesteric texture of MA+7BA; **3.** Canal-like texture of smectic X^* phase in MA+5BA; **4.** Smooth multicolored mosaic-like texture of smectic G^* phase of MA+5BA; **5.** Field-induced phase transition texture of $E_{1.}$; **6.** Optical extinction in E_2 phase.

phase sequence of the various homologues of MA + nBA series in cooling and heating runs can be shown as:

$$\text{Isotropic} \rightarrow \text{G}^* \leftrightarrow \text{Crystal} \quad (\text{MA} + \text{nBA},\ n = 2,\ 3 \text{ and } 4)$$

$$\text{Isotropic} \rightarrow \text{Sm X}^* \leftrightarrow \text{Crystal} \qquad (\text{MA} + 5\text{BA}, \text{MA} + 6\text{BA})$$

$$\text{Isotropic} \rightarrow \text{Ch} \leftrightarrow \text{Crystal} \qquad (\text{MA} + 7\text{BA})$$

$$\text{Isotropic Ch} \rightarrow \text{Sm G}^* \leftrightarrow \text{Crystal} \qquad (\text{MA} + 8\text{BA})$$

Monotropic and enantiotropic transitions are depicted as single and double arrows, respectively.

Fourier Transform Infrared Spectroscopy (FTIR)

FTIR spectra of all the HBFLC complexes are recorded in the solid state (KBr) at room temperature. As a representative case, Fig. 2 illustrates the FTIR spectra of MA + 7BA at room temperature which is discussed elaborately. It is reported [45, 46] that in the alkyl benzoic acids, carboxylic acid exists in monomeric form and the stretching vibration of C=O is observed at 1760 cm^{-1}. A noteworthy feature in the spectrum of the MA + 7BA is the appearance of sharp peak at 1674 cm^{-1} which clearly suggests the dimmer formation, in particular the carbonyl group vibration. [46–49]. A carboxylic acid existing in monomeric form in dilute solution absorbs at about 1760 cm^{-1} because of the electron withdrawing effect. However, acids in concentration solution or in solid state tend to dimerize through hydrogen bonding. It is reported [46] that this dimerization weakens the C=O bond and lowers the stretching force constant K, resulting in a lowering of the carbonyl frequency of saturated acids to $\sim$1710 cm^{-1}. Hence, in the present complexes the formation of H bonding is established by FTIR. A similar trend of result is followed in all the synthesized hydrogen-bonded complexes.

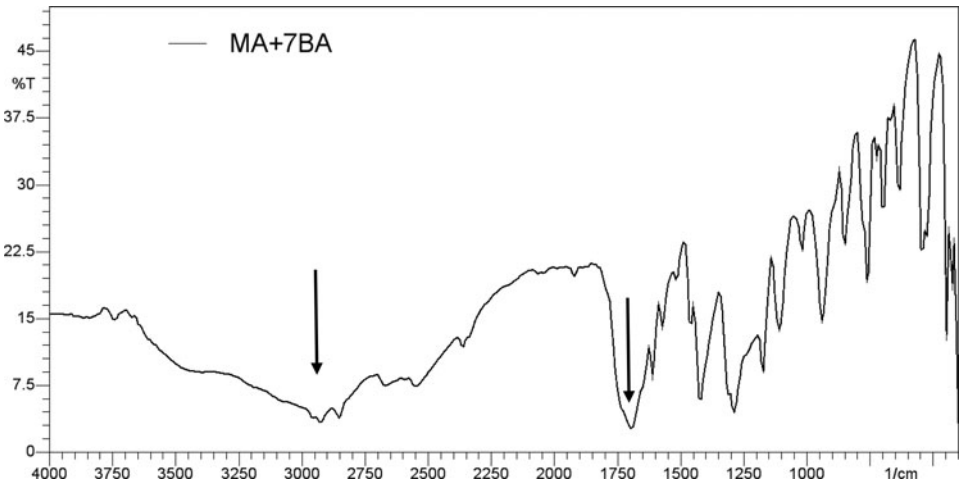

Figure 2. FTIR spectra of MA+7BA complex. Arrows indicate the peaks discussed in the text.

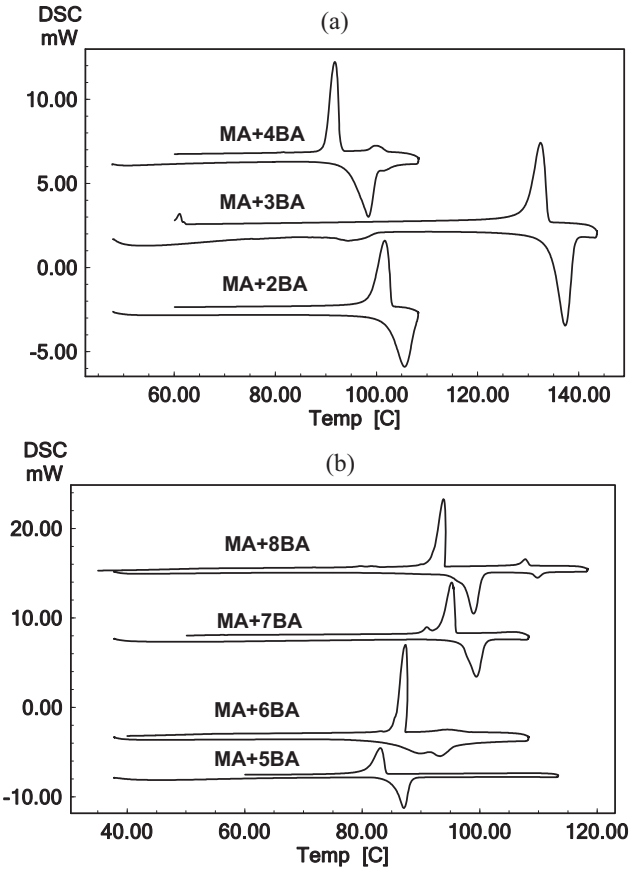

Figure 3. DSC thermograms in (a) heating and (b) cooling cycles of MA+nBA homologous series.

Calorimetric Studies

Differential Scanning Calorimetry

DSC thermograms are recorded in heating and cooling cycle of individual samples. The empty aluminum pan is weighed initially and the desired mesogen is filled to the predetermined weight before crimping it. The crimped aluminum pan along with the sample is placed in the heating chamber of DSC. Another crimped empty aluminum pan is taken as the reference. In the heating chamber, nitrogen gas is purged at a constant rate to create inert environment. DSC thermograms are recorded, stored, and analyzed by TA60 data software. The mesogen is heated with different scan rates viz., 5 °C min^{-1} and 10 °C min^{-1} separately and held at its isotropic temperature for 2 min so as to attain thermal stability. The cooling run is performed with the same scan rate as that of the heating. Experimentally obtained equilibrium transition temperatures and corresponding enthalpy values of the mesogens are listed in Table 1. Fig. 3a and b represents the conventional DSC thermograms obtained for the entire MA+nBA series recorded at a scan rate of 10°C min^{-1}. It can be noticed that transition temperatures obtained by POM studies reasonably concur with the DSC data. From the enthalpy values obtained in the cooling run of the DSC thermograms Cox ratio analysis is performed. The phase transitions from isotropic to cholesteric, cholesteric to

Table 2. Order of phase transitions exhibited by MA+nBA homologous series

Complex	Phase	N_R (ratio)	Order of transition
MA+2BA	G^*	1.40	First
MA+3BA	G^*	1.52	First
MA+4BA	G^*	1.30	First
MA+5BA	X^*	1.35	First
MA+6BA	X^*	1.51	First
MA+7BA	Ch	1.71	First
MA+8BA	Ch	1.53	First
	G^*	1.42	First

smectic X^*, cholesteric to smectic G^*, cholestric to crystal, and smectic G^* to crystal are categorized as first-order transitions (Table 2).

Phase Diagram

Phase diagram of the present homologous series is constructed with POM and DSC data and is illustrated as Fig. 4. Following points can be drawn from the phase diagram.

(i) Phase diagram comprises three chiral phases viz. cholesteric, smectic X^*, and smectic G^*.
(ii) An interesting observation is that all the mesogens of this series are mono-phase variant. An exception to this is MA+8BA which is a bi-phase variant. Yet, another feature is the appearance of higher-ordered smectic G^* phase in the first (MA+2BA) and in the last (MA+8BA) homologues of the series.

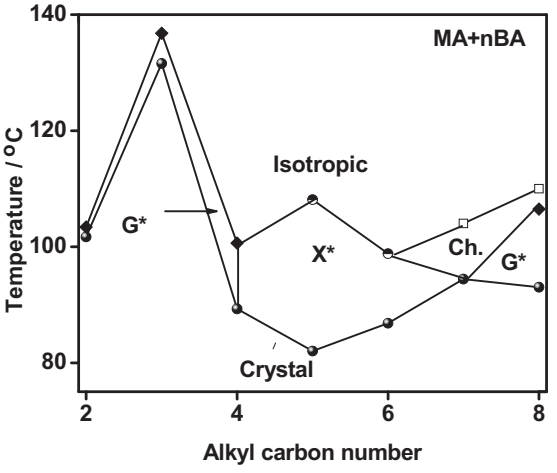

Figure 4. Phase diagram of MA + nBA homologous series.

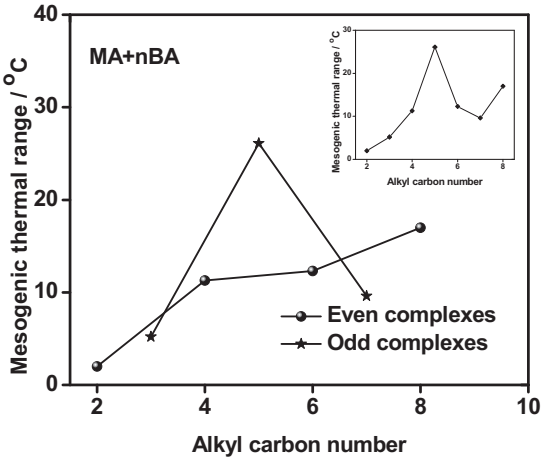

Figure 5. Mesogenic thermal range exhibited by even and odd MA+nBA homologues separately. Insert figure indicates the mesogenic range of all the complexes.

(iii) Mesogenic thermal ranges of the individual complexes are depicted in Fig. 5. To be more precise, mesogenic thermal range possessed by odd alkyl carbon number and even alkyl carbon number are drawn separately (Fig. 5).

(iv) The thermal mesogenic range gradually increased with the increment in the alkyl carbon number. It is maximum for MA + 5BA (26.1°C) and minimum for MA + 2BA (2°C).

(v) New phases have been induced at regular intervals of the alkyl carbon number. In MA + 5BA, smectic G* phase is completely quenched by smectic X* while smectic X* has been completely quenched in MA + 7BA paving way for cholesteric phase. In MA + 8BA, quenching the cholesteric phase, smectic G* reappeared.

(vi) No odd–even effect is observed in the phase transition temperatures. However, isotropic to liquid crystalline phase transition temperature and the liquid crystalline phase to crystal phase transition temperatures are almost unaltered for five complexes viz., MA + 4BA to MA + 8BA.

(vii) Smectic G* is induced in the lower-order homologous series with an exception of MA + 8BA, which may be attributed to the decrease in chain length which makes the molecules more stable exhibiting higher-order phases.

(viii) A new phase labeled as smectic X* is observed in the pentyl and hexyl carbon number homologous series. Further, this phase is sandwiched by isotropic and crystal. Complexes possessing smectic X* phase melt at low temperatures when compared to the other complexes. This clearly shows that the presence of smectic X* phase has drastically reduced the melting temperature. A wide thermal range of smectic X* is noticed in both the complexes viz., MA + 5BA and MA + 6BA.

Thermal Analysis

Thermal law of equilibrium is verified in the DSC thermal analysis cycles viz., total enthalpy values of different phases observed in the heating cycle is equal to the enthalpy values obtained for the same phases in the cooling cycle. In practical considerations, the

Table 3. Sum of enthalpy values obtained in heating and cooling run of DSC thermogram

	DSC Cycles	
Hydrogen-bonded complexes	Σ Enthalpy values of all transitions in heating cycle ($J\ g^{-1}$)	Σ Enthalpy values of all transitions in cooling cycle ($J\ g^{-1}$)
MA+2BA	44.46	41.11
MA+3BA	51.37	49.46
MA+4BA	49.89	44.91
MA+5BA	29.78	29.55
MA+6BA	30.26	33.46
MA+7BA	37.43	36.34
MA+8BA	43.84	43.61

summation of the enthalpy values possessed by the different phases in the heating cycle (endothermic reaction) will be slightly higher than the enthalpy value possessed by the same complex in the cooling cycle (exothermic reaction) (Table 3). Thus the amount of heat evolved is equal to the heat absorbed in the given series.

Thermal Stability and Order of Smectic X Phase Transition*

In order to classify the order of transitions and establish the thermal stability of smectic X*, eleven binary mixtures with empirical formula $A_X\ B_{(1-X)}$ are prepared where A and B represent MA + 6BA and MA + 8BA, respectively, the value X varied from 0% to 100% with a step of 10%. The mesophases exhibited by $A_X\ B_{(1-X)}$ are studied by POM and DSC thermograms. The phase diagram of these binary mixtures constitutes three phases viz., cholesteric, smectic X*, and smectic G* which is presented as Fig. 6.

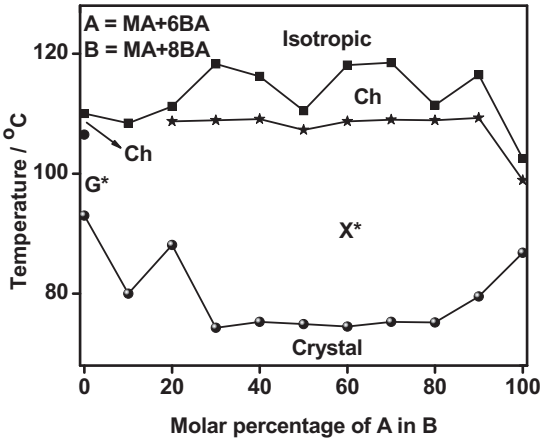

Figure 6. Phase diagram of binary mixtures (MA+5BA and MA+6BA) depicting the growth and stability of Smectic X*.

Table 4. Order of phase transitions exhibited by the different molar concentrations of MA+nBA homologous series

A = MA+6BA B = MA+8BA $[A_{(x)}+B_{(1-x)}]$	Phase	N_R (ratio)	Order of transition*
A = 1, B = 0	Ch	1.49	First
	X*	1.51	First
A = 0.9, B = 0.1	Ch	1.22	First
	X*	1.31	First
A = 0.8, B = 0.2	Ch	1.34	First
	X*	1.46	First
A = 0.7, B = 0.3	Ch	1.54	First
	X*	1.50	First
A = 0.6, B = 0.4	Ch	1.44	First
	X*	1.38	First
A = 0.5, B = 0.5	Ch	1.52	First
	X*	1.53	First
A = 0.4, B = 0.6	Ch	1.36	First
	X*	1.46	First
A = 0.3, B = 0.7	Ch	1.42	First
	X*	1.54	First
A = 0.2, B = 0.8	Ch	1.35	First
	X*	1.38	First
A = 0.1, B = 0.9	Ch	1.35	First
A = 0, B = 1	Ch	1.53	First
	G*	1.42	First

For all the 11 binaries whose molar percentage varied from 0% to 100%, the ratio of the peak magnitudes is evaluated and the data are presented in Table 4. From this data, the order of the transition is deduced and verified by the theory proposed by Navard and Cox [50].

Miscibility Studies: Analysis of Smectic X Thermal Phase Width*

SmecticX* phase is exhibited by MA + 5BA and MA + 6BA complexes which is the mid alkyl carbon chain of the series and the thermal width of this smectic X* phase is reasonably large. In order to study the growth of smectic X* phase, two complexes (MA+6BA and MA + 8BA) of the same homologous series are chosen in such a way that the concentration of MA + 6BA varied from 10% to 90% in MA+8BA. It may be recalled that MA+6BA exhibits smectic X* phase while MA + 8BA does not exhibit smectic X* phase.

The choice of the mesogens can be justified by the following argument. The mesogen MA + 8BA does not exhibit smectic X* phase while MA + 6BA exhibits smectic X* phase. Figure 6 depict the binary phase diagram in which the growth and stabilization of smectic X* are shown. Further the following points can observed from the phase diagram (Fig. 6) and thermal analysis of smectic X* (Fig. 7):

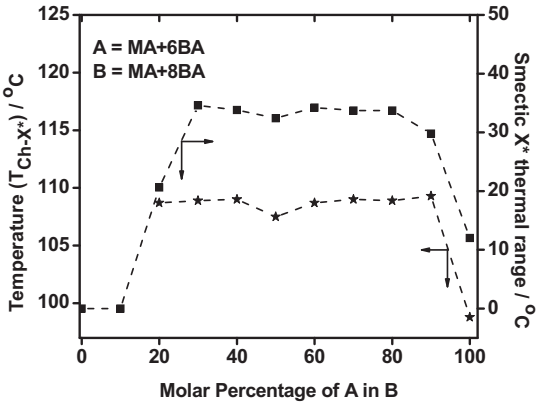

Figure 7. Growth and thermal mesogenic range of smectic X* in MA+5BA and MA+6BA.

(i) Ten percent concentration of MA+6BA in MA + 8BA has not favored inducement of smectic X* phase in 90% of MA + 8BA.
(ii) Molar concentrations of MA + 6BA which varied from 30% to 80% exhibited thermal stabilization of smectic X* phase with unaltered thermal width.
(iii) Increase in the molar percentage of MA + 6BA favored suitable condition for growth of smectic X* phase on the other hand higher-ordered smectic G* phase is observed to be quenched. The threshold value of molar percentage of MA + 6BA to observe smectic X* phase is 20%.
(iv) Smectic X* thermal span is highest (34.6°C) in 30% molar concentration of MA + 6BA in MA + 8BA.
(v) Binary mixtures enhanced mesogenic range in general and smectic X* thermal range in particular compared to its pure counterparts.
(vi) Seventy percent and 80% molar concentration of MA + 6BA in MA + 8BA have the identical thermal range for smectic X* (33.7°C) phase indicating the saturation point beyond which only there is slight decrement.

Helical Pitch Measurement in Smectic X* Phase

In chiralsmectic phase, the helix is formed by a precession of director *n*, around the layer normal. *Z*, the azimuthal tilt direction changes by a small amount when going from layer to layer. Helical pitch is weakly dependent on temperature. It increases slightly with increase in temperature. Helical pitch is measured as reported earlier by us [20, 23]. The sample in smectic X* phase acts as a grating and the measurements of first and second order in the diffraction pattern are carried out. The temperature variation of helical structure in smectic X* phase of MA+5BA is discussed.

The deformation of the helicoidal structure has been experimentally analyzed by varying the temperature. As the temperature is decremented in small steps, the variation of the helix is noted at each step. The variation of normalized helix with temperature is depicted as Fig. 8. The unwinding of the helix with temperature in smectic X* phase indicates that this phase is not only tilted but also possesses helicoidal structure. Canal like texture (plate 3) observed for smectic X* act as grating element and hence when a beam of laser is passed through it, a diffraction pattern is thus observed on the screen.

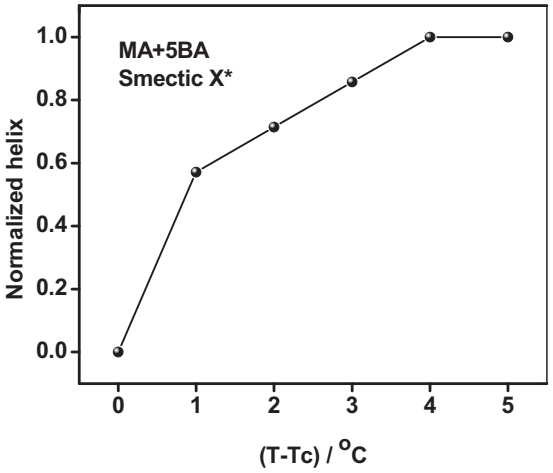

Figure 8. Temperature variation of helical pitch in smectic X* phase of MA+5BA complex.

This diffraction pattern varies with respect to temperature and gets stabilized on further decrement oftemperature.

Tilt Angle in Smectic X* as a Function of Temperature

Temperature variation of tilt angle θ (T) (Fig. 9) in the newly observed phase smectic X* of MA + 5BA and MA + 6BA is measured by optical extinction method [35]. Tilt angle is found to increase with decreasing temperature and attains a characteristic maximum value for both the complexes. The magnitude of tilt angle in smectic X* phase of MA + 5BA at 102.1°C is observed to be 21°55′, while for MA + 6BA, at 92.8°C it is observed to be 22°04′. This larger magnitudes of the tilt angle is attributed to the enhanced orientational disorder introduced by the lengthy flexible part of the molecule, contributing to the observation of a

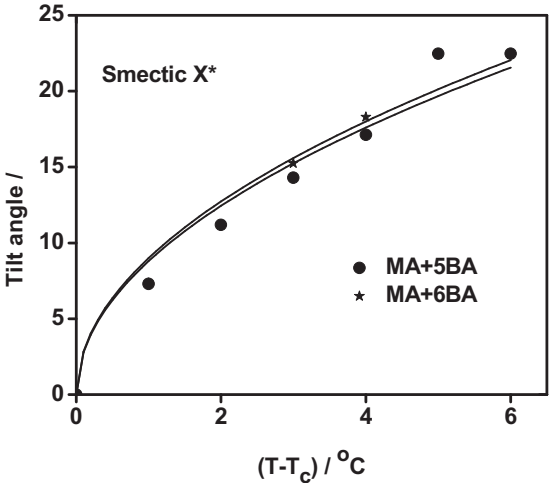

Figure 9. Temperature variation of tilt angle in smectic X* phase in MA+5BA and MA+6BA.

new induced smectic X* phase. Hence, homologues with extended flexible part in HBFLC are argued to contribute positively to the inclined [51] soft covalent hydrogen bonding interaction for the realization of tilted phases of applicational interest.

The observed temperature variation of θ (T) follows a power law relationship given by

$$\theta(T)\alpha(T_C - T)^{\beta} \tag{1}$$

where, T_c represents the transition temperature,

β the critical exponent component value and

T is the temperature at which $\theta(T)$ is experimentally determined.

In Fig. 9, the solid line indicates the theoretical fit drawn by mean field theory and the points over the fitted line are the experimental data points. The estimated value of β for the present members of MA+nBA is found to be in good agreement with the Mean Field theory [52, 53] predicted value, to infer the long-range interaction of transverse dipole moment for the stabilization of tilted smectic X* phase.

P_s Measurement in Smectic X* of MA+5BA and MA+6BA

In MA+5BA and MA+6BA complexes, smectic X* is observed to be a mono variant phase and the thermal span of this phase is found to be 26.1°C and 12 °C, respectively. Complexes are filled in 10 μm spacer cell with an active area of 1 mm^2 and is slowly cooled with polling (ac field of 0.3 V μ^{-1}) from isotropic to smectic X* at a rate of 0.1°C min^{-1} to achieve molecular alignment. Simultaneous textural observations along switching of the molecules are also found to ensure the onset of ferroelectric smectic X* phase.

The spontaneous polarization is experimentally found by current repolarization method [39]. A standard ZLI sample is used for calibration of the setup [40]. The current profiles observed on DSO at various temperatures are digitized with 5000 points and recorded. The sample is excited with a frequency of 30 Hz and field of 0.3 V μ^{-1}. The spontaneous polarization (P_s) is proportional to the area under the curve of the current profiles. The area under the curve is calculated using computer program with an accuracy of 0.01 nC cm^{-2}.

The current profiles are digitized and recorded at various temperatures in smectic X* phase of MA+5BA and MA+6BA. The digitized data is analyzed for evaluation of P_s. Figure 10 illustrates the variation of P_s with temperature in the entire thermal span of smectic X*. The data is fitted to the following power law:

$$P_s(T)\alpha(T_C - T)^{\beta} \tag{2}$$

where, T_c represents the transition temperature from isotropic to smectic X*, β is the critical exponent component value, and T is the temperature at which $P_s(T)$ is experimentally determined.

In Fig. 10, the solid line indicates the theoretical fit drawn by Mean field theory and the points over the fitted line are the experimental data points. As in the case of tilt angle, in the present study also the estimated value of β for the present complexes of MA+nBA is found to be in good agreement with the Mean Field theory [52, 53].

In MA+5BA complex, the magnitude of spontaneous polarization at the onset and offset of the smectic X* are measured to be 0.93 nC cm^{-2} and 3.46 nC cm^{-2}, respectively, and 1.73 nC cm^{-2} and 4.52 nC cm^{-2} for MA+6BA complex. The magnitude of P_s increases gradually with temperature and attained a saturated value. The unwinding of the helix takes place completely, which is understood from the saturation point of P_s value, where the

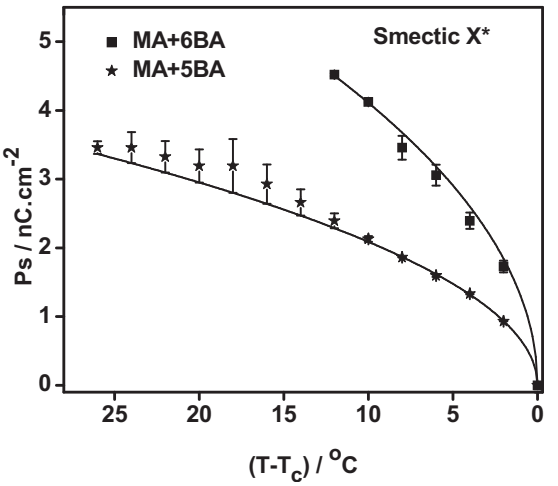

Figure 10. Temperature variation of spontaneous polarization in smectic X* phase of MA+5BA and MA+6BA.

molecules are aligned parallel to the field applied. The higher values of tilt angle in both the mesogens favored the higher magnitudes of spontaneous polarization.

Tilt Angle in Smectic X* as a Function of Applied Fields

Two electrical field-induced transitions are observed in MA+5BA which are designated as E_1 and E_2 with corresponding field values as 0.8 V μ^{-1} and 1.7 V μ^{-1}. The former yields a canal texture as depicted in plate 5 while the latter is optical extinction (plate 6). It is interesting to note that the magnitude of tilt angle in smectic X* and E_1 are strikingly different. In the case of E_2 as there is no texture and hence the measurement of tilt angle does not arise. An attempt is made in analyzing the tilt angle in the smectic X* and E_1 electrical field-induced transition. A field-induced phase transition (smectic X* to E_1) takes place between the field magnitudes of 0 to 0.7 V μ^{-1}.

Tilt angle studies in the smectic X* is discussed below. To study the variation of tilt angle with field in smectic X*, three field values are chosen such that they cover the entire range of smectic X* .Thus, different fields viz., 0 V μ^{-1}, 0.3 V μ^{-1}, and 0.7 V μ^{-1}, are applied to the cell and the tilt angle is measured with respect to temperature and the data are plotted as shown in Fig. 11.

From Fig. 11, it can be clearly observed that at the field of 0.7 V μ^{-1}, a maximum tilt angle of 29° 3′ is observed, while the magnitude of the tilt angle at 0 V μ^{-1} and 0.3 V μ^{-1} are 22° 48′ and 22° 6′, respectively. As expected, the magnitude of tilt angle increases with increase in the field applied. This result enable to understand the free rotation of the molecules and justify the optical shuttering action observed at higher fields which upon increasing the field the molecules inhibited the path of light.

Electric Field-Induced Phase Transition (EFiPT)

A static method [54] i.e., applying d.c field to the liquid crystalline sample at a pre-determined temperature is used to investigate the electric field-induced phase transitions exhibited by the ferroelectric materials (MA+5BA and MA+6BA). Tilt angle, dielectric

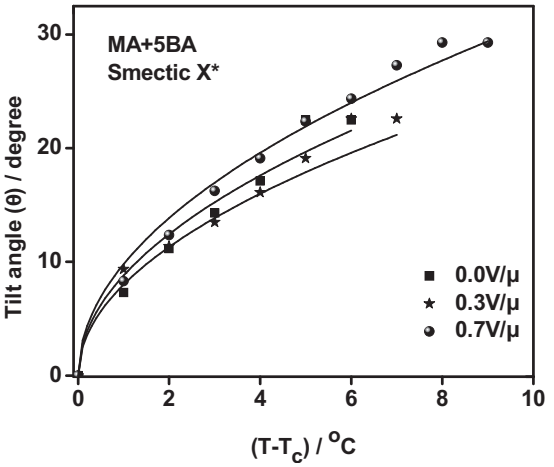

Figure 11. Temperature variation of tilt angle in smectic X* phase of MA+5BA for various applied fields.

spectrum measurements, E–T phase diagram, and spontaneous polarization parameters are measured for the complexes exhibiting smectic X* phase in order to understand the response of the molecules with respect to the applied field.

Tilt Angle Measurement in Smectic X* and E_1 Phases

MA+5BA complex, exhibiting maximum thermal span of smectic X*(26.1°C) phase among the complexes is taken as a representative case and studied in detail. MA+5BA complex is filled uniformly in the polyamide-coated buffed cell and the electrical contacts are drawn from the silver leads. Sample is taken to its isotropic state and the temperature is set to 105.2°C using the Instec standalone temperature controller where the smectic X* phase is fully grown. The applied field is varied in small steps of 0.1 V μ^{-1}, and at each value of the field the corresponding tilt angle is measured. Optical textural observations are also made simultaneously in order to observe the texture of the phase with respect to the applied field. The data is plotted as Fig. 12; from the Fig. 12, it can be seen that the tilt angle increases with increase in the applied field. At 0.8 V μ^{-1}, a drastic variation in the tilt angle is observed which is attributed to the electric field-induced transition labeled as E_1. Further, the corresponding texture of the sample also varied as shown in plate 5. Thus the optical textural observation coupled with the tilt angle measurements enabled to identify field-induced transitions from smectic X* to E_1.

The 0.8 V μ^{-1} field is considered to be the threshold field value for the newly observed electrically induced phase, E_1. Further increment in the magnitude of the field yielded proportional increment in the tilt angle value and the same trend continues till the field value reaches 1.7 V μ^{-1} beyond which the molecules are completely extinct to the path of light (plate 6). Hence, no texture is being observed.

Various electric field-induced phase transitions is depicted below.

$$\text{Smectic X*} \quad \underset{\longleftarrow}{0.8\text{V}/\mu} \quad \text{E}_1 \quad \underset{\longleftarrow}{1.7\text{V}/\mu} \quad \text{E}_2$$

The double arrow indicate that the transitions are reversible on withdrawl of the respective fields.

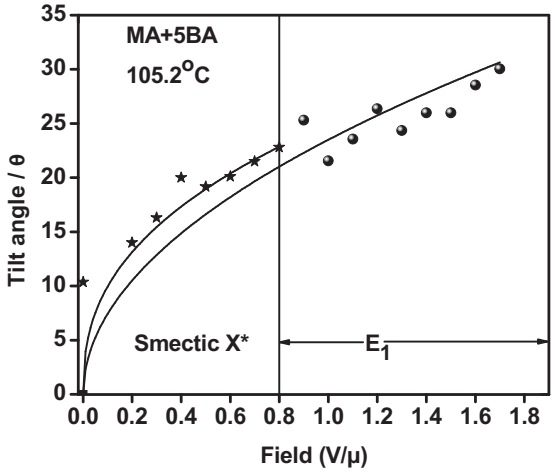

Figure 12. Field variation of tilt angle in smectic X^* and E_1 phases of MA+5BA.

Molecular Modeling

A molecular modeling is proposed for the observed behavior and occurrence of the two electric field-induced phase transitions (Fig. 13). The molecules in both of the field-induced phase E_1 and E_2 are depicted in the model. The tilt angle in the former phase is observed to be around 22° while in the latter it is around 30°. The increment in the tilt angle allows for the inhibition of the polarized light to pass through various smectic layers.

Capacitance and Dielectric Loss Studies in E_1 and E_2 Phases

The molecular orientation which is observed through tilt angle measurements with the applied field influences the capacitance variation and dielectric loss of the sample. As a representative case, results of MA+6BA complex in various field-induced phases are discussed. The sample is studied at 95.3C which is smectic X^* phase. The field is varied in small steps of 0.1 V μ^{-1} and the variation of the capacitance is recorded. The capacitance profile with field is depicted as Fig. 14.

Initially as the field is increased from 0 to 0.5 V μ^{-1}, a linear increment in the capacitance is observed. A steep decrement of the capacitance in the form of an anomaly is observed at 0.8 V μ^{-1} which is attributed to the first field-induced transition, E_1. The simultaneous textural observations also conform the observed fact.

As the magnitude of the field is further increased, the capacitance values increases. As the second field-induced transition approaches a suddenly fall in the magnitude of the capacitance is observed and the light extinction further supports the onset of E_2.

Similar results are observed for dielectric loss measurements which are shown in Fig. 15. Optical tilt angle and dielectric spectrum studies are complimentary to each other (Table 5).

Dielectric Relaxation Studies in E_1 and E_2 Phases

Empty cell with known substance such as benzene is calibrated initially to know the leads capacitance value. Frequency range is scanned by 4192A LF Impedance analyzer and

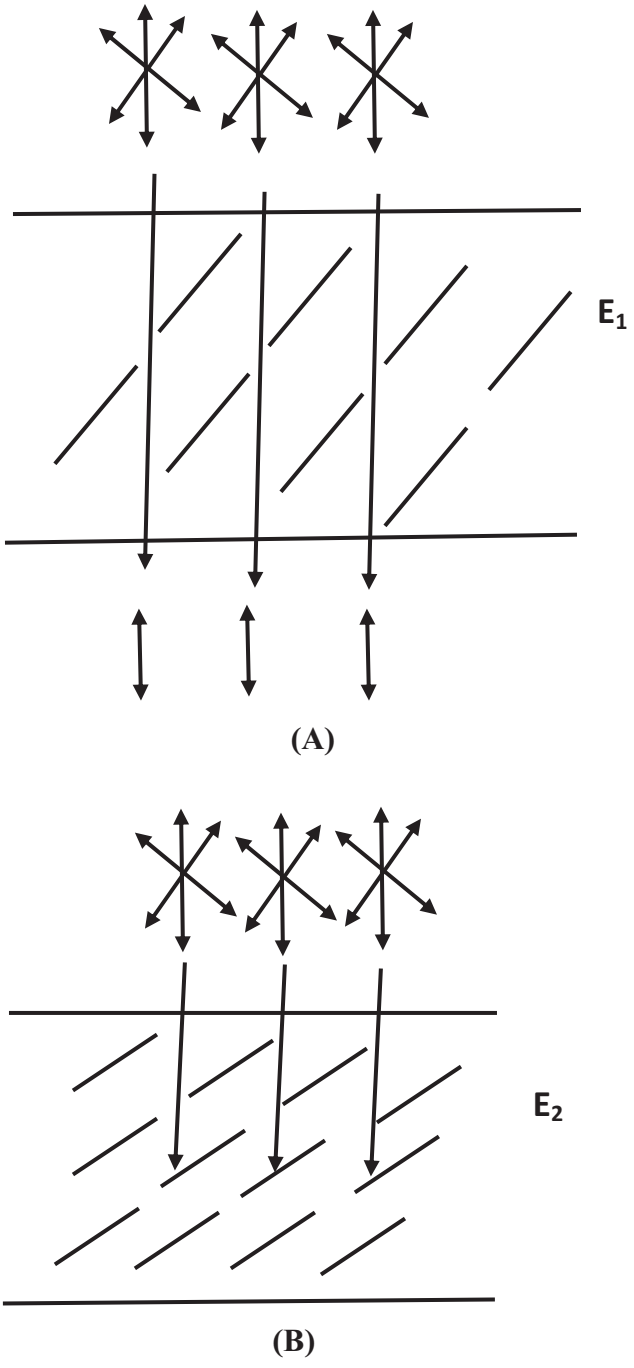

Figure 13. Molecular modeling for optical extinction phenomenon. (A) Light passes through the liquid crystal in E_1 phase (B) Light is inhibited in E_2 phase.

Table 5. Different parameters of field-induced phase transitions observed in MA + nBA complexes

Phase	Threshold field (V μ^{-1})	Tilt angle	Textural observation	ε' (nF)	ε''
Smectic X*	0 – 0.7	21° 55′	Plate 3	0.2037	0.1699
E_1	0.8–1.6	22° 04′	Plates 5 and 6	0.2034	0.1728
E_2	≥1.7	—	Plate 7	< 0.1921	< 0.1671

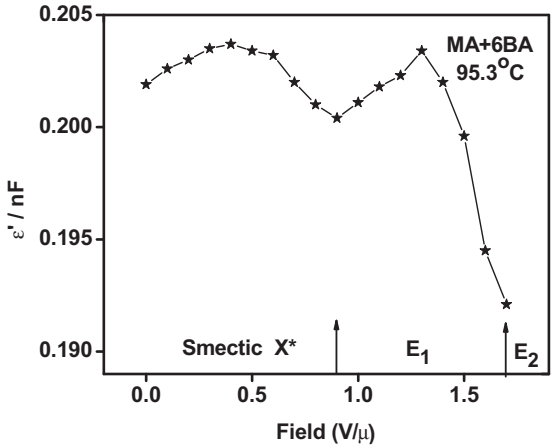

Figure 14. Capacitance profile as a function of applied field in various phases.

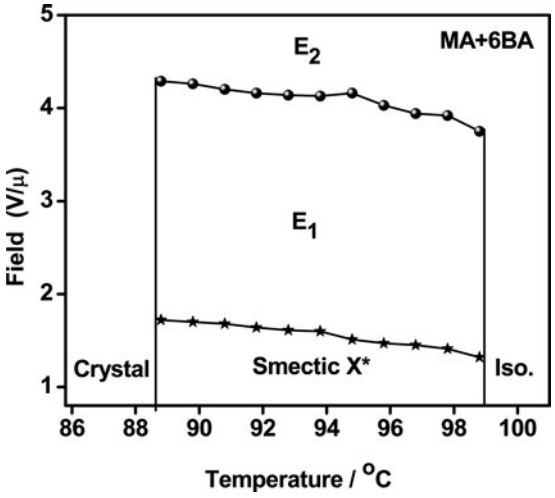

Figure 15. Dielectric loss profile as a function of applied field in various phases.

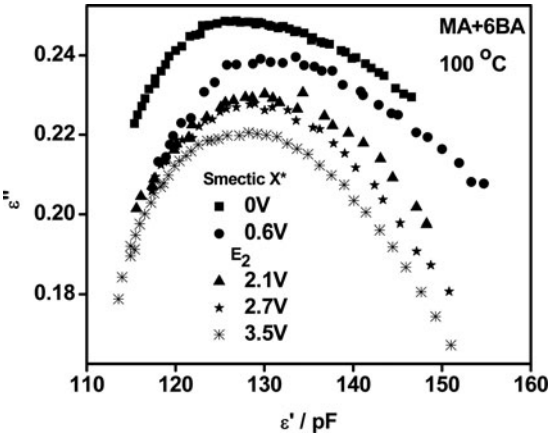

Figure 16. Dielectric dispersion curves obtained in smectic X* and E_2 phases of MA+6BA at 100°C with respect to various applied fields.

the suitable range where the molecules are being relaxed is chosen. Here, for MA+6BA complex, the frequency relaxation range is in between 700 KHz – 1500 KHz. By varying the applied field, corresponding ε' and ε'' values are measured in the smectic X* phase where the temperature is fixed as 100°C. Relative permittivity $\varepsilon'_r(\omega)$ and dielectric loss $\varepsilon''(\omega)$ are calculated by the following equations

$$*\varepsilon'_r(\omega) = \varepsilon'_r(\omega) - j\varepsilon''(\omega)$$
$$\varepsilon'_r(\omega) = [C_{\text{LC}} - C_{\text{leads}}]/[C_{\text{empty}} - C_{\text{leads}}]$$
$$\varepsilon'_r(\omega) = \text{Tan}\delta(\omega) * \varepsilon_r(\omega)$$

The observed variation of dielectric loss with capacitance at 100°C with different applied field is recorded in smectic X* phase and plotted which is referred as dispersion curves (Fig. 16). From the Fig. 16, it can be noticed that as the field is increased the magnitude of dielectric loss decreases. Further, as the field is increased various electric field-induced transitions are clearly noticed with the shift in the relaxation frequency. From the dispersion curves, the magnitude of the dielectric loss is shifted with the temperature for different applied fields. The relaxation frequencies at various fields are calculated from the dispersion curves and plotted as Fig. 17. In smectic X* phase, the relaxation frequencies decrease with the applied field, as the field is further increased in the first field-induced transition, the reverse trend is observed where the relaxation frequencies increase with increased field. Finally, in the second field-induced transition there is a linear increase of the relaxation frequency with applied field. Thus through dielectric relaxation studies, all the three phases viz., smectic X*, E_1, and E_2 are clearly distinguished.

E–T Diagrams

To study the thermal range of field-induced transitions E_1 and E_2, field temperature (E–T) phase diagram is constructed [39, 40] with simultaneous textural observation. For thermal variation of every 1 °C, the magnitude of the field is varied till two threshold values corresponding to E_1 and E_2, field-induced transition, are detected as discussed in the above

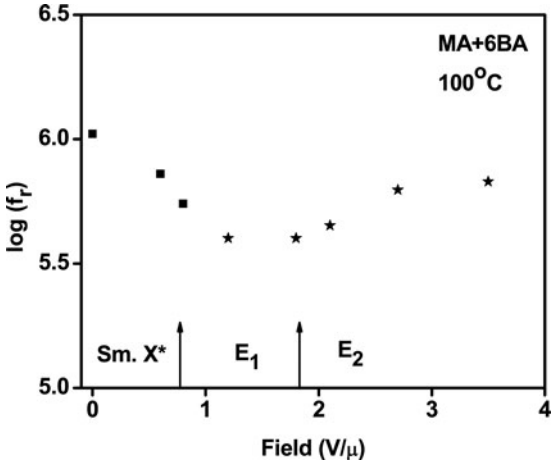

Figure 17. Arrhenius plot of MA+6BA in various phases.

sections. The data obtained for both the field-induced transitions is plotted (Figs. 18 and 19) for two complexes viz. MA+5BA and MA+6BA. The mesogenic range in the former is between 108.1 °C to 82 °C while in the later 98.8 °C to 86.8 °C, respectively. In the above said mesogenic ranges, the field has been varied in small steps from 0 V μ^{-1} to 2.8 V μ^{-1} for MA+5BA and 0V μ^{-1} to 4.5 V μ^{-1} for MA+6BA complexes, respectively.

E–T Diagram of MA+5BA

The E–T diagram of this complex is plotted as Fig. 18 for the entire thermal span of smectic X*, E_1, and E_2 phases. In the complex MA+5BA, the magnitude of the threshold value of E_1, i.e., the transition from smectic X* to E_1 is almost invariant with temperature. The threshold values at 105.2°C is 0.7 V μ^{-1}, while it marginally increased to 1.2 V μ^{-1} at

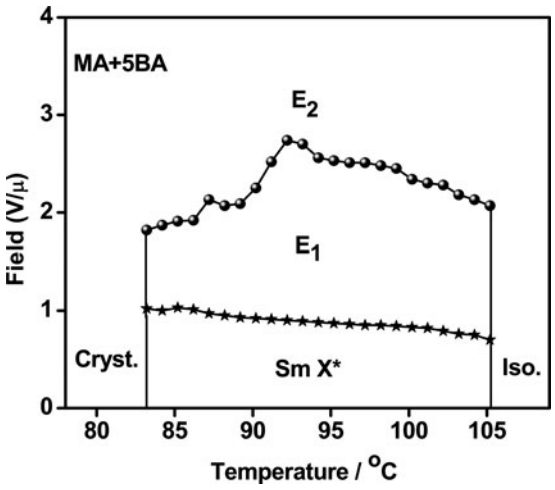

Figure 18. E–T phase diagram of MA+5BA complex.

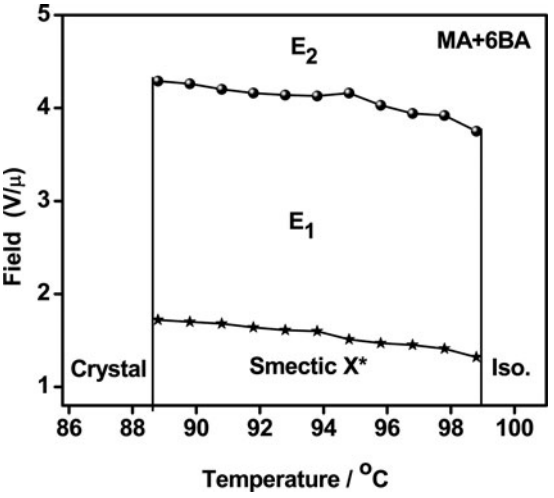

Figure 19. E–T phase diagram of MA+6BA complex.

83.2°C. Thus for a thermal range of 22°C, the increment of threshold value is 0.5 V μ^{-1}, thus the average threshold value is 0.022 V μ^{-1} per one degree change in temperature.

For the second field-induced transition E_2, i.e., the transition from E_1 to E_2, the magnitude of the threshold value increases from 105.2°C to 92.2°C and starts to decrease till 83.2°C, whose threshold field values are found to be 2.07 V μ^{-1}, 2.74 V μ^{-1}, and 1.87 V μ^{-1}, respectively.

E–T Diagram of MA+6BA

The E–T diagram of this complex is plotted as Fig. 19 for the entire thermal span of smectic X*, E_1, and E_2 phases. Here also, the magnitude of the threshold field value of E_1, i.e., transition from smectic X* to E_1 is almost invariant with respect to temperature. Threshold field values at 98.8°C is 1.32 V μ^{-1}, which shows no drastic variation in the magnitude of the field values as the temperature variation proceeds till 88.8°C, where the threshold field value is measured to be 1.72 V μ^{-1}. Thus for a thermal range of 10 °C, the increment of threshold value is 0.4 V μ^{-1}, thus the average threshold value is 0.04 V μ^{-1} per one degree change in temperature.

For second field-induced phase transition E_2, i.e., the transition from E_1 to E_2, the magnitude of the threshold value is almost stabilized as the temperature is decreased from 98.8°C to 88.8°C whose threshold field values are found to be 3.75 V μ^{-1} and 4.29 V μ^{-1}, respectively. This unaltered threshold field values for both the field-induced phase transition E_1 and E_2 declares the stabilization of the formed complex irrespective of the various field applied.

Conclusions

(a) Seven ferroelectric MA+nBA complexes have been designed, synthesized, and characterized, of which two complexes exhibit a new smectic X* phase which is ferroelectric in nature.
(b) Smectic X* is characterized by optical, electrical, and thermal studies.

(c) The order of phase transition and the enhancement of smectic X* phase has been studied by binary mixtures.
(d) Thermal width of smectic X* phase has been studied by miscibility studies.
(e) E–T phase diagram for two complexes is discussed.
(f) Spontaneous polarization, tilt angle, and dielectric spectrum studies are carried out in ferroelectric smectic X* phase.

Acknowledgments

Divine and graceful blessings of Almighty Bannari Amman, infrastructural support rendered by Bannari Amman Institute of Technology (BIT), and the financial support rendered by the Board of Research in Nuclear Sciences (BRNS) of Department of Atomic Energy (DAE), India, (Sanction No. 2012/34/35/BRNS) are gratefully acknowledged by the authors.

References

[1] Brand, H. R., Cladis, P. E., & Pleiner, H. (1992). *Macro. Mol.*, *25*, 7223; Cook, A. G., Baumeister, U., & Tschierske, C. J. (2005). *Mater. Chem.*, *15*, 1708.
[2] Hu, Q. Z., & Jang, C. H. J. (2012). *Mater. Sci.*, *47*, 969.
[3] Kumar, S., & Lakshminarayanan, V. (2004). *Chem. Commun.*, *14*, 1600.
[4] Rajeswari, B. R., Pardhasaradhi, P., Ramakrishna Nanchara Rao, M., Datta Prasad, P. V., Madhavi Latha, D., & Pisipati, V. G. K. M. (2013). *J. Therm. Anal. Calorim.*, *111*, 561.
[5] Suresh, K. A., Yuvaraj Sah, Sunil Kumar, P. B., & Ranganath, G. S. (1994). *Phys. Rev. Lett.*, *72*, 2863.
[6] Yelamaggad, C. V., Achalkumar, A. S., Shankar Rao, D. S., & Krishna Prasad, S. J. (2009). *Org. Chem.*, *74*, 3168.
[7] Srivastava, A., Sa, D., & Singh, S. (2007). *E. P. J. E.*, *22*, 111.
[8] Pardhasaradhi, P., Madhavi Latha, D., Datta Prasad, P. V., Padmaja Rani, G., & Alapati, P. R. (2013). *J. Therm. Anal. Calorim.*, *111*, 1483.
[9] Yazaki, S., Funahashi, M., Kagimoto, J., Ohno, H., & Kato, T. (2010). *J. Am. Chem. Soc.*, *132*, 7702.
[10] Gleeson, H. F., Southern, C. D., Brimicombe, P. D., Goodby, J. W., & Gortz, V. (2010). *Liq. Cryst.*, *37*, 949.
[11] Goodby, J. W., & Leslie, T. M. (1986). United States Patent, 4613209.
[12] Walb, D. M. (1985). United States Patent, 4556727.
[13] Toriyama, K., Nikagomi, T., Sato, H., Fujita, Y., Morita, K., & Arai, Y. (1983). United States Patent, 4372871.
[14] Clark, N. A., & Lager Wall, S. T. (1985). United States Patent, 4367924.
[15] Kato, T., & Frechet, J. M. J. (1989). *J. Am. Chem. Soc.*, *111*, 8533.
[16] Kato, T., & Frechet, J. M. J. (1989). *Macromolecules*, *22*, 3818.
[17] Paleos, C. M., & Tsiourvas, D. (2001). *Liq. Cryst.*, *28*, 1127.
[18] Letellier, P., Ewing, D. E., Goodby, J. W., Haley, J., Kelly, S. M., & Mackenzie, G. (1997). *Liq. Cryst.*, *22*, 609.
[19] Kang, S. K., & Samulski, E. T. (2000). *Liq. Cryst.*, *27*, 371.
[20] Pongali Sathya Prabu, N., Vijayakumar, V. N., & Madhu Mohan, M. L. N. (2011). *J. Mol. Str.*, *994*, 387.
[21] Bruce, D. W. (2008). *Struct. Bond.*, *126*, 161.
[22] Barmatov, E. B., Bobrovsky, A., Barmatova, M. V., & Shibaev, V. P. (1999). *Liq. Cryst.*, *26*, 581.
[23] Kavitha, C., Pongali Sathya Prabu, N., & Madhu Mohan, M. L. N. (2012). *Physica B.*, *407*, 859.
[24] Pongali Sathya Prabu, N., Vijayakumar, V. N., & Madhu Mohan, M. L. N. (2011). *Physica B.*, *406*, 1106.

[25] Pongali Sathya Prabu, N., Vijayakumar, V. N., & Madhu Mohan, M. L. N. (2011). *Phase Transitions*, *85*, 149.
[26] Pongali Sathya Prabu, N., & Madhu Mohan, M. L. N. (2012). *Phase Transitions*, *85*, 592.
[27] Hentrich, F., Diele, S., & Tschierske, C. (1994). *Liq. Cryst.*, *17*, 827.
[28] Kobayashi, Y., & Mtsunage, Y. (1987). *Bull. Chem. Soc. Jpn.*, *60*, 3515.
[29] Pongali Sathya Prabu, N., & Madhu Mohan, M. L. N. (2012). *Mol. Cryst. Liq. Cryst.*, *569*, 72.
[30] Pongali Sathya Prabu, N., & Madhu Mohan, M. L. N. (2013). *J. Mol. Liq.*, *182*, 79.
[31] Kavitha, C., & Madhu Mohan, M. L. N. (2012). *J. P. C. S.*, *73*, 1203.
[32] Kavitha, C., Pongali Sathya Prabu, N., & Madhu Mohan, M. L. N. (2012). *Phase Trans.*, *85*, 973.
[33] Pongali Sathya Prabu, N., & Madhu Mohan, M. L. N. (2013). *Phase Trans.*, *86*, 339.
[34] Pongali Sathya Prabu, N., Pothkuchi, D. M., & Madhu Mohan, M. L. N. (2012). *Physica B.*, *407*, 3709.
[35] Noot, C., Perkins, S. P., & Coles, H. J. (2000). *Ferroelectrics*, *244*, 331.
[36] Pongali Sathya Prabu, N., & Madhu Mohan, M. L. N. (2013). *J. Therm. Anal. Calorim.*, *113*, 811.
[37] Yu, C. J., Kim, W. S., & Lee, S. D. (2004). *Ferroelectrics*, *311*, 77.
[38] Soltani, T., Gharbi, A., Marcerou, J. P., & Gineste, S. (2011). *Eur. Phys. J. Appl. Phys.*, *55*, 10201.
[39] Vaksman, V. M. & Panarin, Yu. P. (1992). *Mol. Mats.*, *1*, 147.
[40] Hoffmann, J., Kuczynski, W., & Malecki, J. (1978). *Mol. Cryst. Liq. Cryst.*, *44*, 287.
[41] Kato, T., & Mizoshita, N. (2002). *Curr. Opin. Solid. State. Mater. Sci.*, *6*, 579.
[42] Kato, T., & Frechet, J. M. J. (1995). *Macromol. Symp.*, *95*, 311.
[43] Kato, T., Frechet, J. M. J., Wilson, P. G., Saito, T., Uryu, T., Fujishima, A., Jin, C., & Kaneuchi, F. (1993). *Chem. Mater.*, *5*, 1094.
[44] Gray, G. W. & Goodby, J. W. G. (1984). *Smectic Liquid Crystals: Textures and Structures*, Leonard Hill: London.
[45] Kato, T., Uryu, T., Kaneuchi, F., Jin, C., & Frechet, J. M. J. (1993). *Liq. Cryst.*, *14*, 1311.
[46] Pavia, D. L., Lampman, G. M., & Kriz, G. S. (2007). *Introduction to Spectroscopy*, Sanat Printers: India.
[47] Nakamoto, K. (1978). *Infrared and Raman Spectra of Inorganic and Co-Ordination Compounds*, Interscience: New York.
[48] Xu, J., Liu, X., Ng, J. K., Lin, T., & He, C. (2006). *J. Mater. Chem.*, *16*, 3540.
[49] Frechet, J. M. J. & Kato, T. (1992). US patent number 139696.
[50] Navard, P., & Cox, R. (1984). *Mol. Cryst. Liq. Cryst.*, *102*, 261.
[51] Yu, L. J. (1993). *Liq. Cryst.*, *14*, 1303.
[52] Chandrasekhar, S. (1992). *Liquid Crystals*, Cambridge University Press: NewYork.
[53] Stanley, H. E. (1971). *Introduction to Phase Transition and Critical Phenomena*, Clarendon Press: New York.
[54] Bahr, C. H., & Heppke, G. (1987). *Liq. Cryst.*, *2*, 825.